

Chemical abundances for Hf 2-2, a planetary nebula with the strongest known heavy element recombination lines

X.-W. Liu¹, M. J. Barlow², Y. Zhang¹, R. J. Bastin², P. J. Storey²

¹ *Department of Astronomy, Peking University, Beijing 100871, P.R. China*

² *Department of Physics and Astronomy, University College London, Gower Street, London WC1E 6BT, UK*

Received:

ABSTRACT

We present high quality optical spectroscopic observations of the planetary nebula (PN) Hf2-2. The spectrum exhibits many prominent optical recombination lines (ORLs) from heavy element ions. Analysis of the H I and He I recombination spectrum yields an electron temperature of ~ 900 K, a factor of ten lower than given by the collisionally excited [O III] forbidden lines. The ionic abundances of heavy elements relative to hydrogen derived from ORLs are about a factor of 70 higher than those deduced from collisionally excited lines (CELs) from the same ions, the largest abundance discrepancy factor (adf) ever measured for a PN. By comparing the observed O II $\lambda 4089/\lambda 4649$ ORL ratio to theoretical value as a function of electron temperature, we show that the O II ORLs arise from ionized regions with an electron temperature of only ~ 630 K. The current observations thus provide the strongest evidence that the nebula contains another previously unknown component of cold, high metallicity gas, which is too cool to excite any significant optical or UV CELs and is thus invisible via such lines. The existence of such a plasma component in PNe provides a natural solution to the long-standing dichotomy between nebular plasma diagnostics and abundance determinations using CELs on the one hand and ORLs on the other.

Key words: ISM: abundances – planetary nebulae: individual: Hf2-2

1 INTRODUCTION

In recent years a number of papers have been published reporting very deep spectroscopic observations of the relatively faint optical recombination lines (ORLs) emitted by heavy element ions in planetary nebulae (PNe), e.g. Liu et al. (1995, 2000, 2001, 2004a,b), Garnett & Dinerstein (2001), Ruiz et al. (2003), Tsamis et al. (2003b, 2004), Peimbert et al. (2004), Sharpee, Baldwin & Williams (2004), Wesson, Liu & Barlow (2005). A common feature of the analyses of these ORLs was that they yielded systematically higher ionic abundances than obtained for the same ions from classical nebular forbidden lines (also known as collisionally excited lines, or CELs). For most PNe, the ORL/CEL abundance discrepancy factors (adf's) typically lie in the range 1.6–3.0, but with a significant tail extending to much higher adf values. Liu et al. (1995) and Luo, Liu & Barlow (2001) found a mean (with respect to all the heavy elements measured) adf of ~ 5 for NGC 7009, while Liu et al. (2000) derived a mean adf of ~ 10 for NGC 6153 and Liu et al. (2001) obtained mean adf's of ~ 6 and 20 for the bulge PNe M 2-36 and M 1-42, respectively. Kaler (1988) reported an extremely strong C II $\lambda 4267$ recombination line from the southern PN

Hf 2-2, with an observed intensity of 9–10 on a scale where $H\beta = 100$, which represents an enhancement of more than a factor of ten compared to most PNe. As part of a search for further high-adf nebulae, we therefore observed Hf 2-2 and report our results here, which confirm that this nebula has the strongest ORLs and highest adf's known for any planetary nebula.

2 OBSERVATIONS

Hf2-2 was observed on three photometric nights in June 2001 with the Boller & Chivens long-slit spectrograph mounted on the ESO 1.52-m telescope. Two wavelength regions were observed. The seeing was between 2–3 arcsec, throughout most of the night of June 18, followed by three nights of sub-arcsec seeing. The slit was positioned at PA = 45° , centred on the central star. The CCD was a 2672×512 Loral UV-flooded chip with a pixel size of $15 \mu\text{m}$ and a read-out-noise of $7.2 e^- \text{pix}^{-1}$ rms.

Two wavelength regions were observed, see Table 1 for a journal of observations. The blue region was observed with

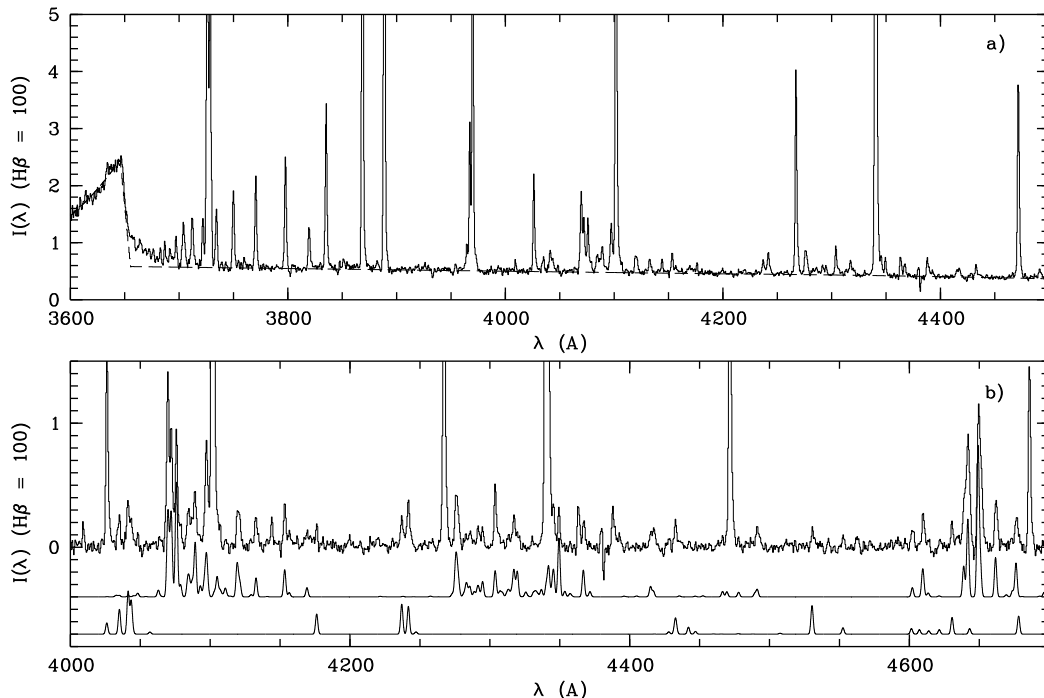


Figure 1. Spectrum of Hf2-2 obtained with the 2arcsec wide slit. The spectrum has been corrected for interstellar reddening and normalized such that H β has an integrated flux of 100. a) $\lambda\lambda$ 3600–4500 showing the huge Balmer jump at 3645 Å that declines steeply towards shorter wavelengths, indicating an average electron temperature of 900 K for the hydrogen recombination spectrum. Overplotted is an empirical fit of the continuum (stellar plus nebular); b) $\lambda\lambda$ 4000–4700 showing the swarm of, often blended, recombination lines from C, N, O and Ne ions. The continuum has been subtracted. Also overplotted are synthesized recombination line spectra of O II (middle curve) and N II (bottom curve), shifted downward by 0.4 and 0.7, respectively. They were calculated assuming $T_e = 900$ K, $\log N_e = 3$ (cm^{-3}), $N(\text{O}^{2+})/N(\text{H}^+) = 7.48 \times 10^{-3}$ and $N(\text{N}^{2+})/N(\text{H}^+) = 2.72 \times 10^{-3}$ (c.f. Table 4).

a 2400 lines mm^{-1} holographic grating, which yielded a dispersion of 32 \AA mm^{-1} , or $\sim 0.5 \text{ \AA pix}^{-1}$. Some vignetting was observed, in particular on the blue side of this large format CCD, which limited the useful wavelength range to 3540–4800 Å. A slitwidth of 2arcsec was used for maximum spectral resolution. In addition, in order to obtain magnitudes for the central star, two spectra with slitwidths of 4 and 8arcsec were also obtained. Because of the UV flooding procedure to maximise sensitivity, the instrumental line width was significantly broader than predicted by the instrumental optics alone – a 2arcsec slit projects to only 1.32pix on the CCD, yet the actual measured line width was about 3pix, or 1.5 \AA FWHM . The spectral resolution degraded even more towards the edges of the spectral coverage, approaching 2 \AA FWHM . The red wavelength region, from 4750–7230 Å, was observed with a 1200 lines mm^{-1} ruled grating at a dispersion of 65.6 \AA mm^{-1} . For a 2arcsec wide slit, this yielded a spectral resolution of 2.8 \AA FWHM including the effects caused by the UV-flooding. All spectra were wavelength-calibrated using exposures of a He-Ar-Ne-Fe lamp and flux-calibrated using 8arcsec wide slit observations of the *HST* standard stars Feige 110 and the central star of the PN NGC 7293. Example spectra obtained with a 2arcsec slitwidth are shown in Fig. 1.

On the night of August 5 2001, an additional spectrum of Hf2-2 was obtained with the IDS Spectrograph mounted on the 2.5-m Isaac Newton Telescope (INT) at La Palma Observatory. The spectrum was obtained with a 316 lines mm^{-1} ruled grating in first spectral order, cov-

Table 1. Journal of observations

Date (UT)	λ -range (Å)	FWHM (Å)	Slit width (arcsec)	Exp. Time (sec)
18/06/01	3550-4800	1.5	2	4×2400
18/06/01	3550-4800	2.6	8	1800
19/06/01	3550-4800	1.5	2	1800
19/06/01	3550-4800	1.9	4	1800
21/06/01	4750-7230	2.8	2	4×1800
21/06/01	4750-7230	5.8	8	1800
05/08/01	4000-7700	8.0	4	600

ering the 4000–7700 Å wavelength range at a resolution of 8 \AA FWHM . A GG385 order sorting filter was used to block out second order light. The CCD was a 4096×512 Loral chip with $13.5 \mu\text{m}$ pixels. A slitwidth of 4arcsec was used. The spectrum was calibrated using observations of the *HST* standard star BD +28° 4211. The INT spectrum was particularly useful for joining the blue and red spectra obtained at ESO without relying on their absolute flux calibration. In addition, the flux of H β in the ESO red spectra was unreliable as it fell close the edge of the spectral coverage and was partially affected by vignetting.

3 ABSOLUTE H β FLUX

Hf2-2 was imaged in the light of [O III] λ 5007 and H α by Schwarz, Corradi & Melnick (1992) during their imaging survey of southern hemisphere PNe. The images were obtained

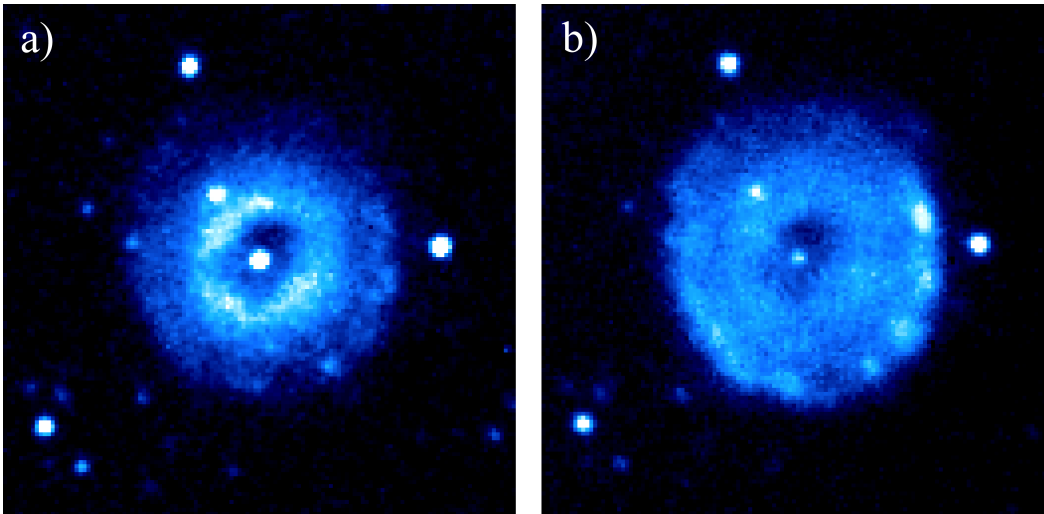


Figure 2. Narrow band images of Hf2-2 in the light of a) [O III] $\lambda 5007$ and b) $H\alpha$, obtained by Schwarz et al. (1992) with the 3.5-m NTT. The field of view is 33.5×33.5 arcsec². North is up and east to the left.

with the BFOCS2 instrument mounted on the 3.5-m New Technology Telescope (NTT), with a spatial sampling of 0.2594 arcsec pix⁻¹. These images are reproduced in Fig. 2. They have been rotated to the normal orientation such that North is up and East to the left. Both the [O III] and $H\alpha$ images show that Hf2-2 is highly symmetric, with an inner disk-like shell and an outer limb-brightened shell that has an angular diameter of 25 arcs. The inner disk (shell) is brighter in [O III] and has a central cavity, which is partially filled at PA = 60° leaving two holes lying symmetrically about the central star.

The ESO red spectra obtained with the 2 and 8 arcsec slitwidths yielded $H\alpha$ fluxes of 5.42 and 23.0×10^{-13} ergs cm⁻² s⁻¹, respectively, after integration along the slit. Since the $H\beta$ fluxes from the ESO red spectra were unreliable due to vignetting, we converted the $H\alpha$ fluxes to those for $H\beta$ using the observed ratio of $F(H\alpha)/F(H\beta) = 4.21$ derived from the INT spectrum, which implies $F(H\beta) = 1.29$ and 5.47×10^{-13} ergs cm⁻² s⁻¹ for the ESO 2 and 8 arcsec slitwidth observations, respectively. To obtain the $H\beta$ flux for the whole nebula, we made use of the $H\alpha$ image of Schwarz et al. We found that our 2 and 8 arcsec slits should have respectively caught 12.5 per cent and 48.8 per cent of the $H\beta$ flux emitted by Hf2-2, implying total $H\beta$ fluxes of 1.03 and 1.12×10^{-12} ergs cm⁻² s⁻¹, or $\log F(H\beta) = -11.99$ and -11.95 (ergs cm⁻² s⁻¹), respectively. We shall adopt $\log F(H\beta) = -11.95$ (ergs cm⁻² s⁻¹) for our analysis, a value which is probably accurate to 0.05 dex.

4 INTERSTELLAR EXTINCTION

The amount of interstellar reddening towards Hf2-2 has to be determined before the observed line fluxes can be used to study the thermal and density structure of the nebula and its elemental abundances. However, apart from its very prominent heavy element ORL spectra, the most striking feature observed in the optical spectrum of Hf2-2 is its very large Balmer continuum jump, accompanied by a steep decline in the continuum intensity on the blue wavelength side

of the discontinuity, indicating a *very* low electron temperature – around 1000 K from a crude estimate, about an order of magnitude lower than the normal value of 10 000 K found in a typical photoionized gaseous nebula. The temperature implied by the Balmer jump is so low that the small but significant dependence of the Balmer line decrement on electron temperature must be taken into account before it can be used to derive the extinction towards Hf2-2.

An initial assessment of the data shows Hf2-2 to be a fairly low density nebula, as indicated by the observed [O II] and [S II] doublet ratios. The extinction towards Hf2-2 also seems to be low. We thus carried out a preliminary plasma diagnostic analysis assuming zero interstellar reddening towards Hf2-2. This yields He⁺/H⁺ and He⁺⁺/H⁺ abundance ratios of 0.127 and 0.002 from the He I $\lambda 4471$ and He II $\lambda 4686$ lines, respectively. These He ionic abundances, together with the observed ratio of the Balmer discontinuity to H 11 of 0.569 \AA^{-1} , yield a Balmer jump electron temperature of $T_e(\text{BJ}) = 890$ K [c.f. Eq. (3) of Liu et al. (2001)]. The observed [O II] $\lambda\lambda 3726, 3729$ and [S II] $\lambda\lambda 6716, 6731$ doublet ratios of 1.43 ± 0.06 and 1.12 ± 0.03 , which are unaffected by reddening, yield electron densities of $\log N_e = 3.1$ and 2.5 (cm⁻³), respectively. In what follows, $T_e = 900$ K and $N_e = 1000$ cm⁻³ will be adopted in order to derive the extinction towards Hf2-2 from a comparison of the observed Balmer decrement with recombination theory (Storey & Hummer 1995) and from the ratio of the observed $H\beta$ to radio free-free fluxes.

The INT spectrum, obtained with a slitwidth of 4 arcsec, yielded an $H\alpha/H\beta$ ratio 4.21, compared to the predicted value of 3.63 for $T_e = 900$ K, yielding a logarithmic extinction at $H\beta$ of $c = 0.20$, for a standard Galactic reddening law (Howarth 1983). Although all of the ESO spectra were obtained under photometric conditions, the blue and red spectra were observed on different nights and the pointing accuracy of the ESO 1.52-m telescope and the positioning of the Boller & Chivens spectrograph long-slit cannot be guaranteed to have repeated exactly on different nights. From the absolute fluxes of $H\gamma$ and $H\alpha$ recorded on the ESO blue and red spectra, respectively ($H\beta$ in the ESO red spec-

Table 2. Observed relative line fluxes, on a scale where $H\beta = 100$

Ident	λ (Å)	$f(\lambda)$	Observed fluxes			Dereddened fluxes		
			2'' slitwidth	4'' slitwidth	8'' slitwidth	2'' slitwidth	4'' slitwidth	8'' slitwidth
Continuum	3643	0.270	2.20	2.04	1.86	2.49	2.31	2.11
Continuum	3678	0.265	0.54	0.45	0.28	0.61	0.50	0.31
H 20	3683	0.264	0.73±0.10	0.74±0.17	0.62±0.10	0.82±0.12	0.84±0.19	0.71±0.11
H 19	3687	0.263	0.92±0.11	0.81±0.17	0.79±0.10	1.04±0.13	0.92±0.20	0.89±0.12
H 18	3692	0.262	0.80±0.11	0.82±0.17	0.87±0.11	0.90±0.12	0.92±0.19	0.98±0.12
H 17	3697	0.262	1.18±0.12	1.25±0.20	0.93±0.11	1.33±0.14	1.41±0.23	1.05±0.12
H16,HeI	3704	0.260	2.18±0.18	2.10±0.30	1.90±0.17	2.45±0.21	2.37±0.33	2.14±0.19
H 15	3712	0.259	2.16±0.17	2.14±0.26	1.88±0.17	2.43±0.19	2.42±0.30	2.12±0.19
H14,[SIII]	3722	0.257	1.65±0.18	1.98±0.32	1.35±0.24	1.86±0.20	2.22±0.36	1.52±0.27
[O II]	3726	0.257	14.48±0.69	14.58±0.42	13.84±1.06	16.29±0.77	16.41±0.48	15.58±1.19
[O II]	3729	0.256	9.75±0.57	10.99±0.38	9.38±1.06	10.97±0.64	12.37±0.43	10.56±1.19
H 13	3734	0.255	2.04±0.13	1.64±0.18	1.74±0.14	2.29±0.14	1.84±0.20	1.96±0.15
H 12	3750	0.253	2.72±0.13	3.13±0.18	2.83±0.13	3.05±0.14	3.51±0.20	3.18±0.14
O III	3760	0.251	0.35±0.14			0.39±0.15		
H 11	3770	0.249	3.03±0.13	2.80±0.18	2.85±0.13	3.40±0.14	3.14±0.20	3.20±0.14
H 10	3797	0.244	3.84±0.13	4.49±0.18	3.58±0.13	4.29±0.14	5.03±0.20	4.01±0.14
He I	3819	0.240	1.53±0.14	1.72±0.18	1.58±0.13	1.71±0.15	1.92±0.20	1.77±0.14
H 9	3835	0.237	5.45±0.13	5.46±0.17	5.42±0.13	6.08±0.14	6.09±0.19	6.05±0.14
[Ne III]	3867	0.231	20.29±0.25	20.18±0.25	19.23±0.25	22.56±0.28	22.45±0.28	21.39±0.28
H8,HeI	3888	0.227	18.81±0.20	17.96±0.30	18.49±0.27	20.88±0.22	19.94±0.33	20.53±0.30
He I	3964	0.211	0.83±0.09	0.78±0.10	0.65±0.16	0.92±0.10	0.86±0.11	0.72±0.18
[Ne III]	3967	0.211	4.37±0.11	4.36±0.12	4.14±0.19	4.82±0.12	4.81±0.13	4.56±0.21
H 7	3970	0.210	12.15±0.16	12.47±0.18	12.68±0.26	13.39±0.17	13.73±0.20	13.97±0.29
He I	4009	0.202	0.31±0.06	0.31±0.08		0.34±0.07	0.35±0.09	
He I	4026	0.198	3.17±0.11	0.31±0.15	3.20±0.11	3.47±0.12	0.34±0.16	3.51±0.12
N II	4035	0.196	0.48±0.06	0.37±0.08	0.31±0.06	0.53±0.07	0.40±0.09	0.34±0.06
N II	4041	0.195	0.72±0.07	0.63±0.09	0.56±0.08	0.79±0.07	0.69±0.10	0.61±0.09
N II	4044	0.194	0.45±0.06	0.33±0.09	0.46±0.08	0.49±0.07	0.36±0.10	0.50±0.09
O II 69.62	4070	0.189	1.06±0.03	1.03±0.05	0.97±0.04	1.15±0.03	1.13±0.05	1.05±0.04
O II 69.89	4070	0.189	1.69±0.05	1.65±0.07	1.54±0.05	1.84±0.06	1.80±0.08	1.68±0.06
O II 72.16	4072	0.188	1.88±0.10	1.82±0.14	1.58±0.12	2.05±0.10	1.98±0.15	1.73±0.13
O II 75.86	4076	0.187	1.85±0.08	1.65±0.12	1.69±0.08	2.02±0.09	1.80±0.13	1.84±0.09
O II 78.84	4079	0.187	0.41±0.07	0.32±0.10	0.36±0.07	0.45±0.08	0.35±0.10	0.39±0.07
O II 83.90	4084	0.186	0.41±0.09	0.30±0.12	0.25±0.10	0.45±0.09	0.32±0.14	0.27±0.11
O II 85.11	4085	0.185	0.39±0.09	0.56±0.13	0.51±0.11	0.42±0.10	0.61±0.14	0.56±0.12
O II 87.15	4087	0.185	0.42±0.07	0.21±0.10	0.20±0.09	0.46±0.08	0.23±0.11	0.22±0.09
O II 89.29	4089	0.184	0.93±0.07	0.90±0.10	0.92±0.08	1.01±0.08	0.98±0.11	1.01±0.08
O II blend	4097	0.183	2.24±0.20	2.03±0.18	1.78±0.35	2.44±0.22	2.21±0.20	1.93±0.38
H I	4101	0.182	21.03±0.55	21.66±0.51	21.77±0.35	22.86±0.60	23.55±0.55	23.67±0.38
O II blend	4120	0.178	0.90±0.10	1.05±0.14	0.91±0.10	0.98±0.11	1.14±0.15	0.99±0.10
O II	4133	0.175	0.56±0.06	0.31±0.07	0.41±0.06	0.61±0.07	0.33±0.08	0.45±0.06
He I	4144	0.172	0.47±0.06	0.42±0.08	0.54±0.06	0.51±0.06	0.45±0.08	0.58±0.07
O II	4153	0.170	0.74±0.07	0.83±0.10	0.84±0.08	0.80±0.08	0.89±0.11	0.91±0.08
O II	4157	0.169	0.27±0.05	0.40±0.08	0.14±0.06	0.30±0.06	0.43±0.08	0.15±0.06
O II	4169	0.167	0.31±0.05	0.19±0.07	0.36±0.05	0.33±0.06	0.21±0.07	0.39±0.06
N II	4176	0.165	0.36±0.05	0.32±0.07	0.35±0.05	0.39±0.06	0.35±0.08	0.38±0.06
NeII blend	4220	0.155	0.22±0.04	0.27±0.07		0.23±0.05	0.29±0.08	
N II blend	4237	0.151	0.61±0.08	0.65±0.13	0.56±0.08	0.65±0.08	0.69±0.14	0.60±0.09
N II blend	4242	0.150	1.00±0.08	0.80±0.12	0.86±0.09	1.07±0.08	0.86±0.13	0.92±0.09
C II	4267	0.144	7.11±0.19	7.09±0.19	6.71±0.15	7.60±0.20	7.58±0.20	7.17±0.16
O II blend	4276	0.142	1.37±0.08	1.44±0.15	1.22±0.10	1.47±0.09	1.53±0.16	1.30±0.10
O II blend	4383	0.117	0.23±0.04	0.30±0.06	0.67±0.10	0.24±0.05	0.31±0.07	0.71±0.10
O II	4286	0.140	0.29±0.04	0.32±0.06		0.31±0.05	0.34±0.07	
O II blend	4292	0.138	0.36±0.05	0.24±0.06	0.86±0.08	0.38±0.05	0.25±0.07	0.91±0.09
O II blend	4295	0.137	0.32±0.04	0.36±0.06		0.34±0.05	0.38±0.07	
O II blend	4304	0.135	1.00±0.06	1.02±0.10	1.24±0.09	1.07±0.07	1.09±0.10	1.32±0.10
O II + ?	4306	0.135	0.23±0.05	0.24±0.07		0.25±0.05	0.26±0.07	
O II blend	4317	0.132	0.56±0.05	0.57±0.08	0.78±0.11	0.59±0.05	0.60±0.08	0.83±0.11
O II	4320	0.132	0.26±0.04	0.27±0.07		0.27±0.05	0.29±0.07	
H I	4340	0.127	42.90±1.16	43.22±0.95	42.79±0.53	45.48±1.23	45.82±1.01	45.37±0.56
O II	4346	0.125	0.75±0.08	0.67±0.08	0.58±0.07	0.79±0.09	0.71±0.09	0.62±0.07
O II	4349	0.125	0.62±0.08	0.87±0.09	0.66±0.06	0.65±0.08	0.92±0.09	0.70±0.06
[O III]	4363	0.121	0.70±0.08	0.83±0.09	0.77±0.06	0.74±0.08	0.88±0.09	0.82±0.07
O II	4367	0.120	0.46±0.07	0.69±0.08	0.53±0.06	0.48±0.08	0.73±0.09	0.57±0.06

Table 2. – continued

Ident	λ (Å)	$f(\lambda)$	Observed fluxes			Dereddened fluxes		
			2'' slitwidth	4'' slitwidth	8'' slitwidth	2'' slitwidth	4'' slitwidth	8'' slitwidth
N III	4379	0.118	0.23±0.07	0.31±0.07	0.39±0.05	0.25±0.07	0.33±0.08	0.41±0.06
He I	4387	0.116	0.67±0.08	0.75±0.08	0.91±0.07	0.71±0.08	0.79±0.09	0.96±0.07
Ne II	4392	0.115	0.21±0.07	0.22±0.07	0.29±0.05	0.22±0.07	0.23±0.07	0.31±0.06
O II	4415	0.109	0.26±0.08	0.21±0.07	0.26±0.09	0.27±0.08	0.22±0.07	0.27±0.09
O II	4417	0.109	0.32±0.08	0.23±0.07	0.27±0.08	0.33±0.08	0.24±0.07	0.28±0.09
N II	4433	0.105	0.48±0.07	0.42±0.05	0.48±0.05	0.51±0.07	0.44±0.05	0.51±0.05
He I	4471	0.096	7.54±0.18	7.52±0.15	7.43±0.10	7.88±0.19	7.86±0.15	7.76±0.10
O II, C II	4491	0.091	0.47±0.06	0.45±0.08	0.59±0.08	0.49±0.06	0.47±0.08	0.61±0.08
N II	4530	0.081	0.38±0.05	0.42±0.08	0.37±0.06	0.39±0.06	0.43±0.08	0.38±0.06
N II	4552	0.076	0.22±0.05	0.27±0.06	0.24±0.05	0.23±0.05	0.28±0.07	0.25±0.06
Mg I]	4562	0.073	0.22±0.05	0.27±0.06	0.25±0.05	0.23±0.05	0.27±0.07	0.26±0.06
O II	4602	0.064	0.40±0.09	0.34±0.09	0.33±0.08	0.41±0.10	0.35±0.09	0.34±0.08
O II	4609	0.062	0.66±0.09	0.79±0.10	0.65±0.09	0.68±0.09	0.81±0.10	0.67±0.10
N II	4630	0.057	0.45±0.06	0.57±0.09	0.40±0.06	0.46±0.07	0.59±0.10	0.41±0.06
N III	4634	0.056	0.26±0.06	0.32±0.09	0.28±0.06	0.26±0.07	0.33±0.09	0.29±0.06
O II	4639	0.055	1.03±0.09	1.01±0.12	0.84±0.09	1.05±0.09	1.03±0.12	0.86±0.10
N III	4641	0.054	0.40±0.14	0.14±0.20	0.73±0.16	0.41±0.14	0.14±0.20	0.75±0.17
O II	4642	0.054	2.14±0.35	2.38±0.50	1.63±0.33	2.20±0.36	2.44±0.51	1.67±0.34
N III	4642	0.054	0.05±0.01	0.06±0.02	0.06±0.01	0.05±0.01	0.07±0.02	0.06±0.01
O II	4649	0.052	2.68±0.13	2.62±0.17	2.68±0.14	2.75±0.13	2.68±0.17	2.75±0.14
O II	4651	0.052	1.23±0.13	1.10±0.16	0.86±0.16	1.26±0.13	1.13±0.16	0.88±0.16
O II	4662	0.049	1.04±0.07	1.19±0.11	0.94±0.06	1.06±0.07	1.22±0.11	0.96±0.06
O II	4674	0.046	0.08±0.00	0.07±0.00	0.08±0.00	0.08±0.00	0.07±0.00	0.08±0.00
O II	4675	0.046	0.42±0.02	0.39±0.02	0.43±0.02	0.43±0.02	0.40±0.02	0.44±0.02
N II	4678	0.045	0.31±0.06	0.16±0.09	0.29±0.06	0.32±0.07	0.17±0.09	0.29±0.06
He II	4686	0.043	3.13±0.10	3.06±0.17	2.73±0.11	3.19±0.10	3.13±0.17	2.78±0.11
He I	4713	0.036	0.48±0.05	0.42±0.10	0.52±0.06	0.49±0.05	0.43±0.10	0.53±0.06
H I	4861	0.000	100.00		100.00	100.00		100.00
He I	4921	-0.015	2.83±0.26		2.66±0.20	2.81±0.26		2.64±0.20
[O III]	4959	-0.024	61.70±0.40	63.90±3.62	62.40±2.00	61.02±0.40	63.20±3.58	61.71±1.98
[O III]	5007	-0.036	191.00±2.00	198.00±3.63	197.00±4.47	187.88±1.97	194.74±3.57	193.78±4.40
He I	5015	-0.038	3.08±0.14		↑	3.03±0.14		↑
[N I]	5200	-0.083	1.37±0.10		1.42±0.10	1.32±0.10		1.37±0.10
C II	5342	-0.117	0.33±0.09		0.29±0.09	0.31±0.09		0.27±0.08
[Cl III]	5517	-0.154	0.26±0.06		0.37±0.09	0.25±0.06		0.34±0.09
[Cl III]	5537	-0.157	0.14±0.05			0.13±0.04		
N II	5667	-0.180	0.63±0.05		0.83±0.09	0.58±0.05		0.77±0.08
N II	5676	-0.181	0.29±0.05		0.18±0.15	0.27±0.05		0.16±0.13
N II	5680	-0.182	1.14±0.07		1.56±0.14	1.05±0.06		1.43±0.13
N II	5686	-0.183	0.29±0.04		0.22±0.08	0.26±0.04		0.21±0.07
N II	5710	-0.187	0.26±0.04		0.19±0.06	0.24±0.04		0.18±0.06
[N II]	5754	-0.194	1.43±0.07		1.23±0.08	1.31±0.06		1.12±0.07
He I	5876	-0.215	32.80±0.30	39.10±2.75	33.30±0.90	29.71±0.27	35.41±2.49	30.17±0.82
[O I]	6300	-0.282	0.66±0.09		0.87±0.22	0.58±0.08		0.76±0.20
[S III]	6312	-0.283	0.35±0.08		0.44±0.22	0.31±0.07		0.38±0.19
[O I]	6363	-0.291	0.19±0.08		0.16±0.16	0.17±0.07		0.14±0.14
C II	6462	-0.306	0.85±0.08		0.92±0.20	0.74±0.07		0.80±0.18
[N II]	6548	-0.318	15.00±0.70	18.80±3.98	15.00±0.70	12.96±0.60	16.24±3.44	12.96±0.60
H I	6563	-0.320	421.00±8.00	421.00±7.48	421.00±16.0	363.29±6.90	363.31±6.46	363.29±13.8
[N II]	6584	-0.323	47.90±1.30	58.60±4.12	46.40±1.40	41.28±1.12	50.50±3.55	39.98±1.21
He I	6678	-0.336	9.72±0.16		9.81±0.18	8.33±0.14		8.40±0.15
[S II]	6716	-0.342	5.76±0.16		5.66±0.13	4.92±0.14		4.84±0.11
[S II]	6731	-0.344	5.18±0.17		5.00±0.13	4.42±0.15		4.27±0.11
He I	7065	-0.387	2.70±0.24		3.11±0.19	2.26±0.20		2.60±0.16
[Ar III]	7135	-0.396	7.70±0.25		7.52±0.20	6.42±0.21		6.27±0.17

tra was unreliable due to vignetting), we derive reddening constants $c = 0.20$ and 0.09 from the 2 and 8 arcsec slitwidth observations, respectively. Note that in this particular nebula, the O II ORLs are so strong that approximately 2 per cent of the observed flux of H γ is due to several O II lines that are blended with it.

Compared to the small reddening implied by the ob-

served INT H α /H β ratio (consistent with the values derived from the H α /H γ ratios from the ESO blue and red spectra, relying on the absolute flux calibration), the fluxes of higher order Balmer lines in the ESO blue spectra, H 9 λ 3835, H ϵ λ 3970 and H δ at λ 4101, relative to H γ , yield consistently higher extinction values – from the 2 arcsec slit observations, we find $c(\text{H}\beta) = 0.67$, 0.67 and 0.72 from the

H γ /H β , H ϵ /H γ and H δ /H γ ratios, respectively. Given the short baseline in wavelength, these values are sensitive to small errors in the measured line ratios – even in the case of H γ /H β , a 5 per cent uncertainty in the ratio translates into an error of 0.2 in $c(\text{H}\beta)$, the consistently higher reddening derived from these high order Balmer lines compared to that yielded by the H α /H β ratio is difficult to explain by observational uncertainties alone. One possibility is that part of the extinction seen towards Hf 2-2 is local and those grains have a steeper extinction curve at shorter wavelength compared to the standard curve for the diffuse interstellar medium. Kaler (1988) derived a value of $c(\text{H}\beta) = 0.88 \pm 0.06$ from the observed ratios of high order Balmer lines relative to H β . Kaler’s observations were obtained at very large air-masses. Nonetheless, for $T_e = 10^4$ K as assumed by Kaler, the higher order Balmer lines measured in our spectra yield an average $c(\text{H}\beta) = 0.82$, almost identical to Kaler’s value.

The radio free-free continuum flux of Hf 2-2 at 1.4 GHz has been measured by Condon & Kaplan (1998), who give $S(1.4 \text{ GHz}) = 4.4 \pm 0.4 \text{ mJy}$. This, together with the total H β flux of $\log F(\text{H}\beta) = -11.95$ ($\text{ergs cm}^{-2} \text{ s}^{-1}$) derived in the previous subsection, and the He ionic abundances given above, yields a reddening constant of $c(\text{H}\beta) = 0.50$. Given the uncertainties in the derived total H β flux and in the radio continuum flux, this value for the reddening constant is probably only accurate to 0.1 dex¹.

We will adopt $c(\text{H}\beta) = 0.20$ for our analysis. The small uncertainties in the amount of reddening towards Hf 2-2 hardly affect our analysis given that most of the ORL diagnostic lines used have wavelengths close to H β . The interstellar extinction maps of Schlegel, Finkbeiner & Davis (1998) predict $E(B - V) = 0.33$ for the direction towards Hf 2-2, corresponding to $c(\text{H}\beta) = 0.47$, implying that Hf 2-2 lies less than half-way along the Galactic dust column in this direction.

5 PROPERTIES OF THE CENTRAL STAR

Hf 2-2 has an unusual central star (CS) – Lutz et al. (1998) have reported it as a photometric variable, with a period of 0.398571 days, though no further information is available. To estimate the magnitude of the CS at the time of our observations, we made use of the blue and red spectra obtained with slitwidths of 4 and 8 arcsec, respectively. The blue spectrum obtained with an 8 arcsec slitwidth was not used as it was obtained under very poor seeing conditions.

In spite of the sub-arcsec seeing conditions under which the two blue and red spectra were obtained, due to the poor tracking accuracy of the ESO 1.52-m telescope and its guiding system, the FWHM of the CS at 3930 Å and 5100 Å in the slit direction as determined directly from the spectra

¹ This interpretation of the H β to the radio continuum flux ratio as a reddening diagnostic is actually questionable, given the extremely peculiar thermal structure of Hf 2-2, as indicated by the enormous difference between the electron temperatures derived from the hydrogen Balmer jump and from the [O III] forbidden line ratio. In Hf 2-2, the Balmer jump temperature is so low that the hydrogen optical continuum emission ($\propto T_e^{-1.5}$), optical line emission ($\propto T_e^{-0.8}$) and radio continuum emission ($\propto T_e^{-0.5}$) could have significantly different average emission temperatures.

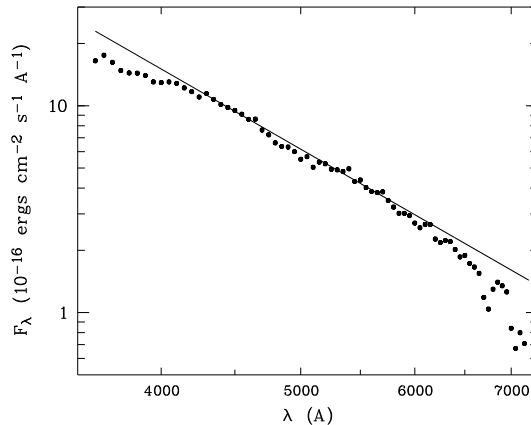


Figure 3. Spectrum of the central star binned in wavelength steps of 50 Å. The solid line shows the energy distribution of a 67,000 K blackbody.

were found to be 2.7 and 3.2 pixels, or 2.2 and 2.6 arcsec, respectively. Nine CCD rows centred on the CS, equivalent to a width of 7.3 arcsec, were co-added to obtain the integrated spectra of the CS. The blue and red spectra overlap between 4750–4810 Å, where the continuum level of the red spectrum is found to be 37 per cent higher than that of the blue spectrum. We therefore multiplied the blue spectrum flux-levels by 1.37 so that the blue and red spectra joined smoothly. To obtain the fluxes for the CS alone, we need however to correct for the contribution from the underlying nebular emission to the extracted CS spectrum.

If the physical conditions (electron temperature, density and the He ionic abundances relative to H⁺) in the ionized region where the nebular continuum emission originates are known, as well as the reddening towards the nebula, the contribution of nebular continuum emission to the integrated central star spectrum can be calculated and then subtracted with the aid of recombination theory. One uncertainty in this approach is the unknown efficiency of the H I two-photon emission, which is an important source of nebular continuum emission shortwards of 4000 Å. Here we have opted to correct for the nebular continuum emission to the integrated CS spectrum by using the nebular spectrum sampled directly from the bright nebular shell. Unfortunately, a field star, at a distance of 5.11 arcsec from the CS at PA = 32.6°, fell into our 4 and 8 arcsec slits positioned at PA = 45°, contaminating the continuum spectrum of the north-east parts of the nebula. The field star is about 1.4 mag fainter than the CS in the [O III] image obtained by Schwarz et al. Thus only the south-west nebular region was used. Three CCD rows, sampling the nebula 3.8 to 7.0 arcsec from the CS were co-added. The resultant blue and red spectra were scaled, using H γ and H α , respectively, to the corresponding line fluxes seen in the extracted CS spectra and then subtracted from the latter.

After correcting for the underlying nebular continuum emission in the integrated CS spectra, residual emission from some nebular emission lines, including the prominent C II and O II recombination lines, is present in the corrected CS spectrum, suggesting that the intensities of these lines relative to H I Balmer lines, are stronger towards the nebular centre. Similarly, some residual Balmer continuum emission

was present shortwards of the 3646 Å limit, indicating that the central regions of the nebula may have a lower Balmer jump temperature. Spatial variations of the nebular properties will be discussed in detail in the next section.

No spectral features are found that can be attributed to the CS. The CS blue and red spectra were merged and binned in wavelength steps of 50 Å. The resulting spectrum is plotted in Fig. 3. The observed fluxes at 4400 and 5500 Å are 10.4 and 4.4×10^{-16} ergs cm⁻² s⁻¹ Å⁻¹. After convolving the spectral energy distribution (SED) with standard B- and V-band response curves, we found B = 17.04 and V = 17.37 and a colour index B - V = -0.33 (Kaler 1988 derived B = 17.5 and V = 18.2). The observed color index is comparable with values found for the hottest *unreddened* stars, indicating that the extinction towards the CS of Hf 2-2 is negligibly small, $E_{B-V} \leq 0.1$, or equivalently $c \leq 0.15$, which is consistent with the very low reddening derived from the H α /H β ratios in §4.

Our measured central star flux of $F(\lambda 5500) = 4.4 \times 10^{-16}$ ergs cm⁻² s⁻¹ Å⁻¹, combined with the dereddened nebular H β flux of 1.78×10^{-12} ergs cm⁻² s⁻¹, yields a blackbody H I Zanstra temperature of 56,000 K, while the above combined with the He II $\lambda 4686$ /H β dereddened flux ratio of 0.028 measured with the 8 arcsec slit implies a blackbody He II Zanstra temperature of 67,000 K. If we had instead dereddened the stellar V magnitude using $c(\text{H}\beta) = 0.20$, corresponding to $A_V = 0.43$, we would have obtained H I and He II Zanstra temperatures of 50,000 K and 64,000 K, respectively. That the He II Zanstra temperature is higher than the H I Zanstra temperature, is consistent with this low-density nebula being optically thin in the H I Lyman continuum.

In Fig. 3, we have plotted the SED of an unreddened blackbody of 67,000 K, normalized to the observed SED of the CS of Hf 2-2 at 5500 Å. The two SEDs agree well with each other between 4200–6500 Å. The decline of the observed SED beyond 6500 Å is clearly caused by the very low S/N at these long wavelengths, and the sharp drop of fluxes near 7000 Å is due to absorption by the telluric atmospheric a- and B-band (at 7160 and 6867 Å, respectively). There is however a significant departure of the observed SED from that of a 67,000 K blackbody shortwards of 4200 Å, suggesting higher extinction than at longer wavelengths, which is in line with the higher reddening derived from the ratios of higher order Balmer lines to H γ . It seems to us that the discrepancy between the reddenings derived from the blue and red wavelength regions is unlikely to be caused by observational uncertainties and is thus probably real.

6 PLASMA DIAGNOSTICS AND ABUNDANCE ANALYSES

6.1 CEL analysis

Table 3 presents electron temperatures derived from the dereddened [O III] ($\lambda 4959 + \lambda 5007$)/ $\lambda 4363$ and [N II] ($\lambda 6548 + \lambda 6584$)/ $\lambda 5754$ nebular to auroral line ratios measured with the different slitwidths, using a mean electron density of 1000 cm⁻³, as derived from the [O II] $\lambda 3729$ / $\lambda 3726$ and [S II] $\lambda 6731$ / $\lambda 6716$ doublet ratios. We adopt $T_e([\text{O III}]) = 8820$ K from the [O III] measurements. The [N II] ratios measured

Table 3. Electron temperatures, densities and ionic and elemental abundances deduced from collisionally excited lines

Diagnostic	Slit width		
	2''	4''	8''
	T_e (K)		
[O III] ($\lambda 4959 + \lambda 5007$)/ $\lambda 4363$	8740	9060	8910
[N II] ($\lambda 6548 + \lambda 6584$)/ $\lambda 5754$	14460 ^a		13400 ^b
	N_e (cm ⁻³)		
[O II] $\lambda 3729$ / $\lambda 3726$	1600	1200	1600
[S II] $\lambda 6731$ / $\lambda 6716$	360		330
	$10^6 \times \text{N}^+/\text{H}^+$		
[N II] $\lambda \lambda 6548, 6584$	9.74	12.0	9.50
	$\text{N}/\text{H} = 5.89 \times 10^{-5}$		
	$10^5 \times \text{O}^+/\text{H}^+$		
[O II] $\lambda \lambda 3726, 3729$	2.13	2.25	2.04
	$10^4 \times \text{O}^{++}/\text{H}^+$		
[O III] $\lambda \lambda 4959, 5007$	1.05	1.09	1.08
	$\text{O}/\text{H} = 1.28 \times 10^{-4}$		
	$10^5 \times \text{Ne}^{++}/\text{H}^+$		
[Ne III] $\lambda \lambda 3868, 3967$	3.60	3.60	3.42
	$\text{Ne}/\text{H} = 4.20 \times 10^{-5}$		
	$10^7 \times \text{S}^+/\text{H}^+$		
[S II] $\lambda \lambda 6716, 6731$	3.46		3.38
	$10^6 \times \text{S}^{++}/\text{H}^+$		
[S III] $\lambda \lambda 6312$	1.25		1.53
	$\text{S}/\text{H} = 2.32 \times 10^{-6}$		
	$10^7 \times \text{Ar}^{++}/\text{H}^+$		
[Ar III] $\lambda \lambda 7135$	7.27		7.10
	$\text{Ar}/\text{H} = 1.34 \times 10^{-6}$		

^a 11,750 K after correcting for the recombination contribution to the observed $\lambda 5754$ line flux; ^b 10,700 K after correcting for the recombination contribution to the observed $\lambda 5754$ line flux.

with the 2 and 8 arcsec slitwidths formally give $T_e([\text{N II}]) = 14,500$ K and 13,400 K, respectively, much higher than the $T_e([\text{O III}])$ values. This is due to a significant contribution by N^{2+} recombination to the $\lambda 5754$ line. Using Eq. (1) of Liu et al. (2000), together with the N^{2+}/H^+ ratio obtained from the N II ORLs (see below, Table 4) and a temperature of 900 K for the recombining ions, we predict a recombination contribution of 0.42, on a scale where H β =100, to the $\lambda 5754$ line, over 30 per cent of its observed intensity. The T_e 's derived from the corrected [N II] ratios are 11,750 K and 10,700 K for spectra taken with the 2 arcsec and 8 arcsec slitwidths, respectively. Given the significant contamination by recombination of the $\lambda 5754$ line, we will not use $T_e([\text{N II}])$ for our subsequent analysis. Since the O^{3+} ion is not expected to have a significant abundance in Hf 2-2, we do not expect that the [O III] $\lambda 4363$ line is affected by a recombination contribution.

Ionic and elemental abundances derived from CELs using $T_e = 8820$ K and $N_e = 1000$ cm⁻³ and ionization correction factors (icf's) taken from Kingsburgh & Barlow (1994) are presented in Table 3.

6.2 ORL analysis

Plasma diagnostics and an abundance analysis using recombination lines and continuum are presented in Table 4. Electron temperatures have been derived from the ratio of the Balmer discontinuity at 3646 Å to H 11 of the H I spec-

Table 4. Electron temperatures and ionic and elemental abundances deduced from recombination lines and continuum

Diagnostic	Slit width		
	2''	4''	8''
		T_e (K)	
BJ/H 11	930	875	910
He I $\lambda 5876/\lambda 4471$	940	< 550	720
He I $\lambda 6678/\lambda 4471$	1170		1000
O II $\lambda 4089/\lambda 4649$	630	630	630
		He ⁺ /H ⁺	
He I $\lambda 4471$	0.102	0.102	0.101
He I $\lambda 5876$	0.103	0.122	0.104
He I $\lambda 6678$	0.099		0.100
Adopted	0.102		0.102
		He ⁺⁺ /H ⁺	
He I $\lambda 4686$	0.0018	0.0018	0.0016
		He/H = 0.104	
		C ⁺⁺ /H ⁺	
C II $\lambda 4267$	3.68×10^{-3}	3.66×10^{-3}	3.47×10^{-3}
C II $\lambda 5342$	2.98×10^{-3}		2.60×10^{-3}
C II $\lambda 6462$	3.21×10^{-3}		3.47×10^{-3}
Adopted	3.68×10^{-3}	3.66×10^{-3}	3.47×10^{-3}
		C/H = 4.27×10^{-3}	
		N ⁺⁺ /H ⁺	
N II $\lambda 5667$	2.48×10^{-3}		3.29×10^{-3}
N II $\lambda 5676$	2.60×10^{-3}		1.54×10^{-3}
N II $\lambda 5680$	2.41×10^{-3}		3.28×10^{-3}
N II $\lambda 5686$	3.34×10^{-3}		2.70×10^{-3}
N II $\lambda 5710$	4.64×10^{-3}		3.48×10^{-3}
N II Mult. V 3	2.66×10^{-3}		3.04×10^{-3}
N II $\lambda 4630$	2.17×10^{-3}	2.78×10^{-3}	1.93×10^{-3}
N II Mult. V 5	2.17×10^{-3}	2.78×10^{-3}	1.93×10^{-3}
N II $\lambda 4035$	3.19×10^{-3}	2.40×10^{-3}	2.05×10^{-3}
N II $\lambda 4041$	2.78×10^{-3}	2.43×10^{-3}	2.15×10^{-3}
N II $\lambda 4044$	2.11×10^{-3}	1.55×10^{-3}	2.15×10^{-3}
N II $\lambda 4176$	2.89×10^{-3}	2.59×10^{-3}	2.81×10^{-3}
N II $\lambda 4237$	4.61×10^{-3}	4.89×10^{-3}	4.26×10^{-3}
N II $\lambda 4242$	5.66×10^{-3}	4.55×10^{-3}	4.87×10^{-3}
N II $\lambda 4433$	4.71×10^{-3}	4.06×10^{-3}	4.71×10^{-3}
N II $\lambda 4530$	2.04×10^{-3}	2.25×10^{-3}	1.99×10^{-3}
N II $\lambda 4552$	5.40×10^{-3}	6.57×10^{-3}	5.67×10^{-3}
N II $\lambda 4678$	2.64×10^{-3}	1.40×10^{-3}	2.40×10^{-3}
N II 3d – 4f	3.33×10^{-3}	2.90×10^{-3}	2.97×10^{-3}
Adopted	2.72×10^{-3}	2.84×10^{-3}	2.65×10^{-3}
		N ³⁺ /H ⁺	
N III $\lambda 4379$	6.22×10^{-5}	8.21×10^{-5}	1.02×10^{-4}
		N/H = 3.29×10^{-3}	

trum (Liu et al. 2001), from the He I $\lambda 5876/\lambda 4471$ and $\lambda 6678/\lambda 4471$ ratios (Liu 2003; Zhang et al. 2005a,b) and from the O II $\lambda 4089/\lambda 4649$ ratio (Liu 2003; Wesson, Liu & Barlow 2003). The O II temperatures were derived by comparing the observed $\lambda 4089/\lambda 4649$ ratio to theoretical value as a function of temperature calculated down to a temperature of 288 K (c.f. Fig. 7 of Tsamis et al. 2004).

Emissivities of hydrogen recombination lines and continua have only a weak density dependence at electron densities lower than $10,000 \text{ cm}^{-3}$. Given the fairly low density of Hf 2-2, $\sim 1000 \text{ cm}^{-3}$ as indicated by forbidden line density-diagnostics (c.f. Table 3), precise determinations of N_e using ORLs are difficult. Zhang et al. (2004) determined electron temperature and density of H I recombination spectrum

Table 4. – *continued*

Diagnostic	Slit width		
	2''	4''	8''
		O ⁺⁺ /H ⁺	
O II $\lambda 4639$	9.38×10^{-3}	9.20×10^{-3}	7.68×10^{-3}
O II $\lambda 4642$	7.77×10^{-3}	8.62×10^{-3}	5.90×10^{-3}
O II $\lambda 4649$	5.11×10^{-3}	4.98×10^{-3}	5.11×10^{-3}
O II $\lambda 4651$	1.12×10^{-2}	1.01×10^{-2}	7.86×10^{-3}
O II $\lambda 4662$	7.41×10^{-3}	8.53×10^{-3}	6.71×10^{-3}
O II $\lambda 4674$	3.60×10^{-3}	3.15×10^{-3}	3.60×10^{-3}
O II $\lambda 4676$	3.58×10^{-3}	3.33×10^{-3}	3.67×10^{-3}
O II Mult. V 1	6.63×10^{-3}	6.74×10^{-3}	5.74×10^{-3}
O II $\lambda 4320$	3.01×10^{-3}	3.23×10^{-3}	
O II $\lambda 4346$	8.91×10^{-3}	8.01×10^{-3}	6.99×10^{-3}
O II $\lambda 4349$	3.13×10^{-3}	4.42×10^{-3}	3.37×10^{-3}
O II $\lambda 4367$	5.01×10^{-3}	7.63×10^{-3}	5.96×10^{-3}
O II Mult. V 2	4.55×10^{-3}	5.50×10^{-3}	4.82×10^{-3}
O II $\lambda 4415$	7.44×10^{-3}	6.06×10^{-3}	7.44×10^{-3}
O II $\lambda 4417$	1.48×10^{-2}	1.08×10^{-2}	1.26×10^{-2}
O II Mult. V 5	1.02×10^{-2}	7.85×10^{-3}	9.39×10^{-3}
O II $\lambda 4072$	7.43×10^{-3}	7.17×10^{-3}	6.27×10^{-3}
O II $\lambda 4076$	5.06×10^{-3}	4.51×10^{-3}	4.61×10^{-3}
O II $\lambda 4079$	1.07×10^{-2}	8.33×10^{-3}	9.29×10^{-3}
O II $\lambda 4085$	8.14×10^{-3}	1.18×10^{-2}	1.08×10^{-2}
O II Mult. V 10	6.43×10^{-3}	6.16×10^{-3}	5.85×10^{-3}
O II $\lambda 4133$	9.24×10^{-3}	5.00×10^{-3}	6.82×10^{-3}
O II $\lambda 4153$	8.48×10^{-3}	9.44×10^{-3}	9.65×10^{-3}
O II $\lambda 4157$	2.00×10^{-2}	2.87×10^{-2}	1.00×10^{-2}
O II $\lambda 4169$	1.03×10^{-2}	6.54×10^{-3}	1.22×10^{-2}
O II Mult. V 19	9.84×10^{-3}	8.97×10^{-3}	9.16×10^{-3}
O II $\lambda 4084$	7.82×10^{-3}	5.56×10^{-3}	4.69×10^{-3}
O II $\lambda 4087$	8.57×10^{-3}	4.28×10^{-3}	4.10×10^{-3}
O II $\lambda 4089$	5.10×10^{-3}	4.95×10^{-3}	5.10×10^{-3}
O II $\lambda 4276$	6.03×10^{-3}	6.27×10^{-3}	5.33×10^{-3}
O II $\lambda 4304$	1.05×10^{-2}	1.07×10^{-2}	1.29×10^{-2}
O II $\lambda 4286$	8.25×10^{-3}	9.04×10^{-3}	
O II $\lambda 4602$	1.21×10^{-2}	1.03×10^{-2}	1.00×10^{-2}
O II $\lambda 4609$	8.00×10^{-3}	9.53×10^{-3}	7.88×10^{-3}
O II 3d – 4f	7.22×10^{-3}	6.96×10^{-3}	6.63×10^{-3}
Adopted	7.48×10^{-3}	7.03×10^{-3}	6.93×10^{-3}
		O/H = 8.62×10^{-3}	
		Ne ⁺⁺ /H ⁺	
Ne II $\lambda 4392$	2.28×10^{-3}	2.38×10^{-3}	3.21×10^{-3}
Ne II $\lambda 4220$	4.29×10^{-3}	5.40×10^{-3}	
Ne II 3d – 4f	2.99×10^{-3}	3.46×10^{-3}	3.21×10^{-3}
Adopted	2.28×10^{-3}	2.38×10^{-3}	3.21×10^{-3}
		Ne/H = 3.28×10^{-3}	

by simultaneously fitting the observed Balmer discontinuity and high-order Balmer lines for a large sample of Galactic PNe. For Hf 2-2, they obtained $T_e(\text{BJ}) = 1000 \pm 400 \text{ K}$ and $\log N_e = 2.6 \pm 0.5 \text{ cm}^{-3}$ using the 2 arcsec wide slit spectrum presented here. The temperature is slightly higher, but agrees within the uncertainties, with the values presented in Table 4, obtained using Eq. (3) of Liu et al. (2001). Fig. 4 plots the variation of the He I $\lambda 5876/\lambda 4471$ and $\lambda 6678/\lambda 4471$ line ratios as a function of T_e for different electron densities. The observed ratios of Hf 2-2 indicate that the He I recombination lines must arise from ionized regions with $N_e \lesssim 10^5 \text{ cm}^{-3}$.

Liu (2003) first used the intensity ratios of the O II 3d $^4\text{F}_{9/2} - 3\text{p}^4\text{D}_{7/2}^o$ $\lambda 4076$ (Multiplet V 10) and $3\text{p}^4\text{D}_{7/2}^o - 3\text{s}^4\text{P}_{5/2}$ $\lambda 4649$ (Multiplet V 1) lines, the strongest recom-

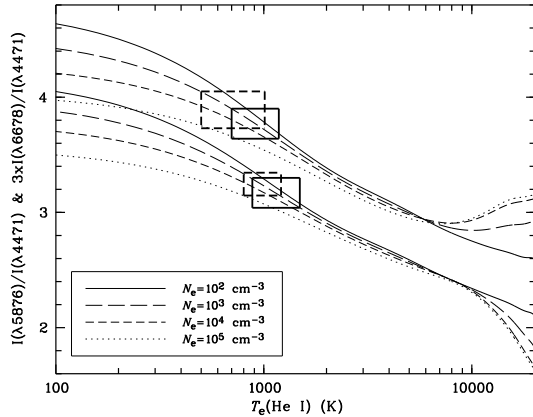


Figure 4. Ratios of He I $\lambda 5876/\lambda 4471$ (the upper set of four curves) and $3 \times \lambda 6678/\lambda 4471$ (the lower set of curves) as a function of T_e for different electron densities. The observed ratios for Hf 2-2 and the implied temperatures (assuming $N_e = 1000 \text{ cm}^{-3}$) are marked using dashed-line and solid-line boxes for spectra obtained with the 2 and 8 arcsec slitwidths, respectively. The sizes of the boxes correspond to the measurement uncertainties.

bination lines from the $3d - 3p$ and $3p - 3s$ electron configurations, respectively, to the $4fG[5]_{11/2}^o - 3d^4F_{9/2}$ $\lambda 4089$ line, the strongest transition from the $4f - 3d$ configuration, to determine the *average* electron temperature under which the lines emitted by Hf2-2 arise. This presented the first direct evidence that they originate from ionized regions with temperatures lower than 1000 K. On the other hand, Liu (2003) notes that the intensities of other weaker transitions from the $3d - 3p$ and $3p - 3s$ configurations, such as the $3d^4F_{7/2} - 3p^4D_{5/2}^o$ $\lambda 4072$ and $3p^2D_{5/2}^o - 3s^2P_{3/2}$ $\lambda 4415$ lines, appear to be too strong by $\approx 0.1 - 0.2$ dex compared to the $\lambda 4089$ line, yielding higher O II emission temperatures. Liu (2003) attributed this to underpopulation of the $2p^2^3P_2$ level of the recombining O^{2+} ions relative to the thermal equilibrium value under low nebular densities and suggested that this effect can be used to measure the *average* electron density under which the recombination lines arise. Further evidence pointing to the underpopulation of the $2p^2^3P_2$ level of O^{2+} at low densities is presented by Tsamis et al. (2003a) in their analysis of Galactic and Magellanic Cloud H II regions.

Calculations of effective recombination coefficients that take into account the populations of the individual fine-structure levels of the recombining ion have now been carried out and preliminary results reported by Bastin & Storey (2005). In Fig. 5 we show the relative intensities of seven of the eight components of multiplet V 1 as a function of electron density, from the *ab initio* intermediate coupling calculation of effective recombination coefficients described by Bastin & Storey (2005). Also shown are the observed relative intensities from the 2, 4 and 8 arcsec slitwidth observations, positioned at the density that gives the best fit to the theory for the strongest five components in each case. The best fit electron densities are 4850, 4000 and $13,500 \text{ cm}^{-3}$ for the 2, 4 and 8 arcsec slitwidth data, respectively. The electron densities derived from the CELs are significantly lower, ranging from 330 to 1600 cm^{-3} and, as can be seen from Fig. 5, in strong disagreement with the observed intensity ratios in multiplet V 1. We note that the theoretical

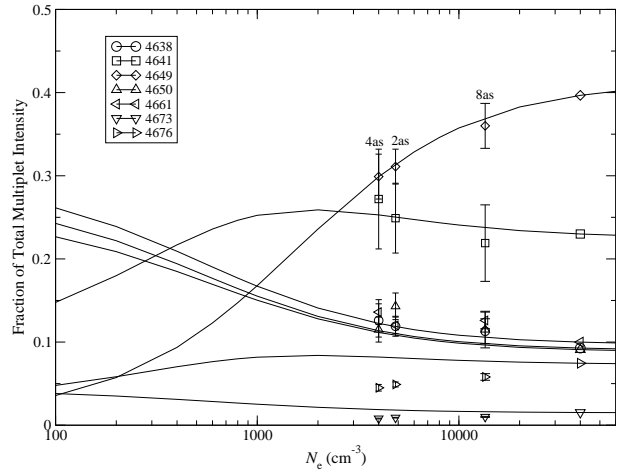


Figure 5. Relative intensities of the components of O II multiplet V 1 as a function of electron density from theory (solid lines) and observations with 2, 4 and 8 arcsec slits. The density is varied to obtain the best fit for the five strongest lines.

intensities shown in Fig. 5 were calculated at $T_e = 10^4 \text{ K}$ (Bastin & Storey, 2005) while the recombination line He I and O II recombination line intensities suggest that an electron temperature closer to 10^3 K may be more realistic for the ORL-emitting region. The theoretical relative intensities are expected to be only weakly dependent on temperature in the range $10^3 - 10^4 \text{ K}$ so the conclusions about the density of the ORL-emitting region is expected to remain valid at the lower temperature. Note that the upper levels of the O II $\lambda 4089$ and $\lambda 4649$ lines have the same $O^{2+} 2p^2^3P_2$ level as parent, so the effect of density on their intensity ratio, and consequently the O II ORL temperature deduced from it, is minimal.

An empirical calibration of the intensity of the $3p^4D_{7/2}^o - 3s^4P_{5/2}$ $\lambda 4649$ transition relative to the total intensity of the whole multiplet V 1 as a function of *forbidden line* electron density has also been given by Ruiz et al. (2003). A more recent calibration, treating H II regions and PNe separately, was given by Peimbert & Peimbert (2005). Using their calibration for PNe, we estimate an average electron density of $N_e \lesssim 10^4 \text{ cm}^{-3}$ for the O II ORL emission regions in Hf 2-2 in broad agreement with the results of the *ab initio* calculation.

The ionic abundances presented in Table 4 were derived assuming an electron temperature $T_e = 900 \text{ K}$ and density $N_e = 1,000 \text{ cm}^{-3}$ for all ionic species – hydrogen, helium and heavy elements inclusive. If we assumed $T_e = 630 \text{ K}$ for heavy element ions, as deduced from the O II $\lambda 4089/\lambda 4649$ ratio, and $T_e = 900 \text{ K}$ for H^+ , the resultant ionic abundances of heavy elements are reduced by less than 10 per cent compared to those tabulated in Table 4. Note that for Ne^{++}/H^+ , only effective recombination coefficients calculated for a nominal temperature of $10,000 \text{ K}$ are available for the $3d - 4f$ transitions. Hence the Ne^{++}/H^+ ionic abundances presented in Table 4 should be treated as quite preliminary.

Table 5. Spatial variations

Quantity	NE2	NE1	Cent	SW1	SW2
CEL analysis					
$T_e([\text{O III}])$ (K)		8750	9900	8510	
$N_e([\text{O II}])$ (cm^{-3})	1290	1990	2550	1890	860
$N_e([\text{S II}])$ (cm^{-3})	380	340	840	450	320
$10^4 \times \text{O}^+/\text{H}^+$	0.155	0.210	0.240	0.210	0.213
$10^4 \times \text{O}^{++}/\text{H}^+$	0.851	1.25	1.17	1.21	0.732
$10^4 \times \text{O}/\text{H}$	1.01	1.46	1.41	1.42	0.945
N^+/O^+	0.641	0.315	0.329	0.304	0.770
ORL analysis					
$T_e(\text{BJ})$ (K)	1030	870	810	780	1220
$T_e(\lambda 5876/\lambda 4471)$ (K)	810	620	910	550	730
$T_e(\lambda 6678/\lambda 4471)$ (K)	950	900	900	1010	1520
He^+/H^+	0.099	0.102	0.101	0.103	0.100
$\text{He}^{++}/\text{H}^+$		0.002	0.004	0.002	
He/H	0.099	0.104	0.105	0.105	0.100
$10^3 \times \text{C}^{++}/\text{H}^+$	2.34	4.22	5.42	3.91	1.66
$10^3 \times \text{O}^{++}/\text{H}^+$	3.22	6.03	9.70	6.75	3.30
$\text{C}^{++}/\text{O}^{++}$	0.726	0.701	0.559	0.579	0.504

6.3 Spatial variations

Given the faintness of the nebula, only limited information regarding the spatial variations of electron temperature, density and elemental abundances can be retrieved from the current data set. We divided the nebula into five regions: 1) NE2 (from $-10.2 < r \leq -6.1$ arcsec, where r is the nebular radius measured along the slit from the north-east to the south-west, c.f. Fig. 2); 2) NE1 ($-6.1 < r \leq -2.0$ arcsec); 3) Centre ($-2.0 < r \leq 2.0$ arcsec); 4) SW1 ($2.0 < r \leq 6.1$ arcsec); and 5) SW2 ($6.1 < r \leq 10.2$ arcsec). Only spectra obtained with the 2 arcsec slitwidth at the ESO 1.52-m telescope were analyzed. The results are presented in Table 5. The first part of the Table presents quantities derived from the CEL analysis, with consecutive rows giving, respectively, electron temperatures derived from the $[\text{O III}]$ ($\lambda 4959 + \lambda 5007$)/ $\lambda 4363$ nebular to auroral line ratio, electron densities deduced respectively from the $[\text{O II}]$ $\lambda 3729/\lambda 3726$ and $[\text{S II}]$ $\lambda 6731/\lambda 6716$ doublet ratios, ionic abundances O^+/H^+ and O^{++}/H^+ derived respectively from intensities of the $[\text{O II}]$ $\lambda \lambda 3726, 3729$ lines relative to $\text{H}\gamma$ and of the $[\text{O III}]$ $\lambda \lambda 4959, 5007$ lines relative to $\text{H}\alpha$, total elemental abundances O/H (sums of O^+/H^+ and O^{++}/H^+), and the ionic abundance ratios N^+/O^+ with N^+/H^+ determined from intensities of the $[\text{N II}]$ $\lambda \lambda 6548, 6584$ lines relative to $\text{H}\alpha$. All CEL ionic abundances were calculated assuming a constant electron temperature of 8820 K and an electron density of 1000 cm^{-3} . The $[\text{O III}]$ $\lambda 4363$ auroral line was too faint to be detectable for regions NE2 and SW2. Compared to regions NE1 and SW1, the central region has an $[\text{O III}]$ temperature about 1000 K higher. From the outer regions to the centre, we see an increase in electron density by a factor of two. The total elemental abundance ratio O/H varies by only 40 per cent from region to region. Given the sensitivity of ionic abundance ratios deduced from CELs to small errors in temperature, the small variations of O/H are likely to be caused entirely by measurement uncertainties, in particular those in temperature determinations. Similarly, the slightly higher N^+/O^+ ratios (which, to a good approximation, $\sim \text{N}/\text{O}$) found for the two outermost regions are probably not real.

Table 6. Comparison of elemental abundances

Source	He	C	N	O	Ne	S	Ar
Hf 2-2 CELs			7.77	8.11	7.62	6.36	6.13
Hf 2-2 ORLs	11.02	9.63	9.52	9.94	9.52		
Av. PNe ^a	11.06	8.74	8.38	8.66	8.06	6.99	6.51
Solar ^b	10.90	8.39	7.83	8.69	7.87	7.19	6.55

^a Average abundances of Galactic disk and bulge PNe (Kingsburgh & Barlow 1994; Exter, Barlow & Walton 2004), all based on CEL analyses except for helium for which ORLs were used; ^b Solar values from Lodders (2003)

In the second part of Table 5, we present plasma diagnostics and ionic and elemental abundances deduced from ORLs. The consecutive rows give, respectively, the electron temperatures derived from the ratio of the H I Balmer jump to H 11, the temperatures derived respectively from the He I $\lambda 5876/\lambda 4471$ and $\lambda 6678/\lambda 4471$ ratios, the ionic abundances He^+/H^+ and $\text{He}^{++}/\text{H}^+$ determined respectively from the He I $\lambda \lambda 4471, 5876, 6678$ lines and from the He II $\lambda 4686$ line, total elemental abundances He/H (sums of He^+/H^+ and $\text{He}^{++}/\text{H}^+$), ionic abundance ratios C^{++}/H^+ and O^{++}/H^+ derived respectively from the C II $\lambda 4267$ and O II $\lambda \lambda 4649, 4651$ ORLs, and finally the $\text{C}^{++}/\text{O}^{++}$ ionic abundance ratios. All ionic abundances were calculated assuming a constant electron temperature of 900 K and an electron density of 1000 cm^{-3} . The Balmer jump temperature $T_e(\text{BJ})$ shows a clear trend of decreasing towards the nebular centre, whereas no clear trends are found for the He I temperatures, which are however extremely difficult to measure, given the very weak dependence of the line ratios on temperature. In dramatic contrast to the O/H abundance ratios deduced from CELs, both C^{++}/H^+ and O^{++}/H^+ (which, after multiplying by a *constant* factor of 1.18, c.f. Table 5, should be very good approximations, within 10 per cent, to C/H and O/H , respectively) show large enhancements towards the nebular centre, by as much as a factor of three, with $\text{C}^{++}/\text{O}^{++}$ ($\approx \text{C}/\text{O}$) varying by less than ~ 40 per cent. Previous analyses of NGC 6153 (Liu et al. 2000), NGC 6720 (Garnett & Dinerstein 2001) and NGC 7009 (Luo & Liu 2003) also showed that ORLs strongly peak towards the nebular centre. This thus seems to be a ubiquitous phenomenon amongst PNe.

7 DISCUSSION

Elemental abundances derived from CELs and from ORLs are compared in Table 6. Also listed in the Table are average abundances for Galactic disk and bulge PNe taken from Kingsburgh & Barlow (1994) and Exter, Barlow & Walton (2004), and the latest solar photospheric values compiled by Lodders (2003).

The oxygen abundance derived from the CELs (8.11 on a logarithmic scale where $\text{H} = 12.00$) is 0.55 dex smaller than the mean value of 8.66 found for Galactic disk and bulge PNe (Kingsburgh & Barlow 1994; Exter et al. 2004). Since it seems unlikely that Hf 2-2 has an abnormally low oxygen abundance, given the great strength of its ORLs, we have explored what physical conditions would be needed to return a more ‘normal’ oxygen abundance from its CELs. We find that the adoption of $T_e = 6560$ K for both the oxygen CELs and the recombining H^+ in the nebula would

yield $\log(\text{O}/\text{H}) + 12.0 = 8.66$, while the adoption of $T_e = 4030$ K would bring the oxygen CEL and ORL abundances into agreement, at $\log(\text{O}/\text{H}) + 12.0 = 9.94$. If we were to adopt the $T_e([\text{O III}])$ of 8820 K for the oxygen CELs but used $T_e(\text{BJ}) = 900$ K, the H I Balmer jump temperature, for H β , then we would find $\log(\text{O}/\text{H}) + 12.0 = 8.88$. However, if H β and the oxygen CELs originate from such physically distinct regions, then an abundance ratio based on their relative intensities is meaningless.

There are two ionic species, doubly ionized oxygen and neon, for which abundances have been determined using both CELs and ORLs. In both cases, the ORL abundance is about a factor of 70 larger than the CEL value. The abundance discrepancy factors (adf's) observed in Hf2-2 are thus the largest for any known PN (except, possibly, the H-deficient knots in Abell30 where the adf's reach nearly three orders of magnitude – c.f. Wesson et al. 2003). Equally remarkable is that Hf2-2 exhibits the lowest Balmer jump temperature, ~ 900 K ever measured for a PN. This is in good agreement with the relation observed in other PNe, i.e. the adf is positively correlated with the difference between the $[\text{O III}]$ forbidden line temperature and the Balmer jump temperature (Liu et al. 2001). The very low Balmer jump temperature of Hf2-2 and its unusually strong heavy element ORLs mimic closely what was found for the ejected shell around nova DQ Her 1934, for which Williams et al. (1978) detected a strong broad emission feature at 3644 Å which they identified as the Balmer jump formed at a very low temperature not exceeding about 500 K.

Ever since the detection of a Balmer jump temperature as low as 3560 K for the Galactic bulge PN M1-42, 5660 K lower than the $[\text{O III}]$ forbidden line temperature measured for the same nebula (Liu et al. 2001), it has become increasingly clear that PNe, at least those exhibiting large adf's, must contain another component of previously unknown ionized gas. This component of gas is a strong ORL emitter yet is essentially invisible in traditional strong CELs, as the electron temperature prevailing there is too low to excite any UV or optical CELs. This is probably caused by the much enhanced cooling by ionic infrared fine-structure lines that is a consequence of a very high metallicity. This inference is supported by detailed photoionization modelling (Péquignot et al 2003; Tylenda 2003) and by direct measurements of the *average* electron temperatures under which various types of line are emitted (c.f. Liu 2003, 2005 for recent reviews). The current observation and analysis add further credibility to this conjecture. In particular we have provided new observational evidence that the electron density of the region emitting the ORLs differs significantly from the CEL emitting region, reinforcing the conclusion that at least two distinct components are involved in a more complete understanding of the ORL/CEL spectra.

PNe are found to show a wide range of adf's, from nearly unity, i.e. agreement between the CEL and the ORL abundances, up to nearly a factor of 100, as in the most extreme case reported here. Two-abundance photoionization modelling of NGC 6153 (Péquignot et al. 2002, 2003), which exhibits an average adf of approximately 10 (Liu et al. 2000), shows that only a few Jupiter masses of gas with a metal overabundance of a factor of 100, are needed to account for the observed intensities of ORLs. In a recent detailed analysis of the He I recombination spectrum of a

large sample of Galactic PNe, Zhang et al. (2005a) concluded that a typical value of 10^{-4} for the filling factor of hydrogen-deficient material is sufficient to explain the systematic difference between the electron temperatures determined from H I recombination spectra and those deduced from the He I ORL ratios. The latter are found to be systematically lower than the former, consistent with the expectations of the two-abundance model but at odds with the traditional paradigms of temperature fluctuations and/or density inhomogeneities.

The volume emissivity of a recombination line is proportional to the product of the densities of the emitting ions and of electrons and increases with decreasing temperature [$\epsilon(X^{i+}, \lambda) \propto N(X^{(i+1)+})N_e T_e^{-\alpha}$, where $N(X^{(i+1)+})$ is the density of recombining ions and $\alpha \sim 1$]. The total mass of H-deficient (metal-rich) material required to produce the observed strengths of ORLs can be determined if one knows the distance to the nebula as well as the electron temperature and density of the emitting gas. The distance to Hf2-2 is poorly known. Cahn & Kaler (1971) and Maciel (1984) gave estimates of 4.0 and 4.5 kpc, respectively, based on the Shklovsky method (Shklovsky 1956). Given the peculiar nature of Hf2-2, the method is unlikely to be valid. Here we have simply adopted a nominal value of 4.25 kpc. If we assume $T_e = 630$ K, $N_e = 5000 \text{ cm}^{-3}$ (c.f. §6.2, Table 4 and Fig. 5), then from the observed intensity of the O II $\lambda 4649$ line, we find a total number of O^{++} ions emitting the $\lambda 4649$ ORL of $N_{\lambda 4649}(\text{O}^{++}) = 4.8 \times 10^{51} (d/4.25 \text{ kpc})^2$, where d is the distance to the nebula in kpc. After correcting for the ionic concentration in O^+ , the total mass of oxygen equals $7.4 \times 10^{-5} (d/4.25 \text{ kpc})^2 M_{\odot}$. For hydrogen, if we assume $T_e = 1000$ K, $N_e = 320 \text{ cm}^{-3}$, as deduced from simultaneously fitting the observed H I Balmer discontinuity and decrement (Zhang et al. 2004), we find $N_{\lambda 4861}(\text{H}^+) = 1.8 \times 10^{55} (d/4.25 \text{ kpc})^2$, or a total mass of ionized hydrogen $1.4 \times 10^{-2} (d/4.25 \text{ kpc})^2 M_{\odot}$. The latter is far less than the nominal total mass of ionized gas of $0.3 M_{\odot}$ for an optically thin PN, even after taking into account the contribution from helium. Similarly, from the $[\text{O III}] \lambda 5007$ forbidden line, assuming $T_e = 8920$ K, $N_e = 1000 \text{ cm}^{-3}$ (c.f. §6.1, Table 3), we find $N_{\lambda 5007}(\text{O}^{++}) = 2.8 \times 10^{51} (d/4.25 \text{ kpc})^2$, or a total mass of oxygen of $4.6 \times 10^{-5} (d/4.25 \text{ kpc})^2 M_{\odot}$. Thus the amounts of metal in the cold H-deficient component and in the hot “normal” component are comparable. If we assume that the $[\text{O III}] \lambda 5007$ forbidden line arises entirely from the hot gas, whereas the O II $\lambda 4649$ recombination line originates exclusively from the cold component, then the total number of oxygen atoms in the nebula is simply the sum of those in the two components. This leads to an average O/H abundance for the *whole* nebula of 5.4×10^{-4} , or, on a logarithmic scale where H = 12.00, O = 8.73, which is almost identical to the solar photospheric value of 8.69. The O/H abundances of the hot and of the cold gas cannot be determined individually unless one knows how to separate the contributions from the two components to the observed total flux of H β .

Two scenarios have been proposed for the possible origins of the postulated H-deficient material (Liu 2003; 2005): 1) nucleo-processed material ejected in a late helium flash as proposed for “born-again” PNe such as Abell30 and 78 (Iben, Kaler & Truran 1983); 2) icy material left over from the debris of planetary system of the progenitor star of the

PN. It is also possible that PNe exhibiting particularly large adf's , including those “born-again” PNe, are related to the phenomenon of novae (Wesson et al. 2003). The last possibility is particularly attractive in view that Hf2-2 is a known close binary system with an orbital period of only 0.398571 days (Lutz et al. 1998) and that the nebula has been suggested to result from a common envelope ejection event (Soker 1997; Bond 2000). Further observations, in particular high spectral and spatial resolution spectroscopic observations using an integral field facility mounted on a large telescope, may prove critical to discriminate between these scenarios.

8 ACKNOWLEDGMENTS

We thank Dr. R. Corradi for providing access to the original [O III] and H α images of Hf2-2 published by Schwarz et al. (1992). We would also like to thank Dr. R. Rubin for a critical reading of the manuscript prior to its publication. The work is partly supported by a joint research grant co-sponsored by the Natural Science Foundation of China and the UK’s Royal Society.

REFERENCES

- Bastin R. J., Storey P. J., 2005, in R. Szczerba, G. Stasinska and S. K. Gorny, eds., *Planetary Nebulae as Astronomical Tools*, AIP Conference Proceedings, Vol 804, p.63
- Bond H., 2000, in J. H. Kastner, N. Soker and S. Rappaport, eds., *Asymmetrical Planetary Nebulae II: From Origins to Microstructures*, ASP Conference Series, Vol. 199, p.115
- Cahn J. H., Kaler J. B., 1971, *ApJS*, 22, 319
- Condon J. J., Kaplan D. L., 1998, *ApJS*, 117, 361
- Exter K. M., Barlow M. J., Walton N. A., 2004, *MNRAS*, 349, 1291
- Garnett D. R., Dinerstein H. L., 2001, *ApJ*, 558, 145
- Howarth I. D., 1983, *MNRAS*, 203, 301
- Iben I., Kaler J. B., Truran J. W., 1983, *ApJ*, 264, 605
- Kaler J. B., 1988, *PASP*, 100, 620
- Kingsburgh R. L., Barlow M. J., 1994, *MNRAS*, 271, 257
- Liu X.-W., 2003, in S. Kwok, M. Dopita and R. Sutherland, eds. *IAU Symp. #209, Planetary Nebulae: Their Evolution and Role in the Universe*. ASP, San Francisco, p.339
- Liu X.-W., 2005, in J. Walsh, L. Stanghellini and N. Douglas, eds., *Proc. ESO Workshop on Planetary Nebulae beyond the Milky Way*. Springer-Verlag, Berlin, in press
- Liu X.-W., Storey P. J., Barlow M. J., Clegg R. E. S., 1995, *MNRAS*, 199, 272, 369
- Liu X.-W., Storey P. J., Barlow M. J., Danziger I. J., Cohen M., Bryce M., 2000, *MNRAS*, 312, 585
- Liu X.-W., Luo S.-G., Barlow M. J., Danziger I. J., Storey P. J., 2001, *MNRAS*, 327, 141
- Liu Y., Liu X.-W., Luo S.-G., Barlow M. J., 2004a, *MNRAS*, 353, 1231
- Liu Y., Liu X.-W., Barlow M. J., Luo S.-G., 2004b, *MNRAS*, 353, 1251
- Lodders K., 2003, *ApJ*, 591, 1220
- Luo S.-G., Liu X.-W., 2003, in S. Kwok, M. Dopita and R. Sutherland, eds. *IAU Symp. #209, Planetary Nebulae: Their Evolution and Role in the Universe*. ASP, San Francisco, p.393
- Luo S.-G., Liu X.-W., Barlow M. J., 2001, *MNRAS*, 326, 1049
- Lutz J., Alves D., Becker A., et al., 1998, *BAAS*, 30, 894
- Maciel W. J., 1984, *A&AS*, 55, 253
- Peimbert A., Peimbert M., 2005, *RevMexAA (Serie de Conf.)*, 23, 9.
- Peimbert M., Peimbert A., Ruiz M. T., Esteban C., 2004, *ApJS*, 150, 431
- Péquignot D., Amara M., Liu X.-W., Barlow M. J., Storey P. J., Morisset C., Torres-Peimbert S., Peimbert M., 2002, *RMxAA (Conf. Ser.)*, 12, 142
- Péquignot D., Liu X.-W., Barlow M. J., Storey P. J., Morisset C., 2003, in S. Kwok, M. Dopita and R. Sutherland, eds. *IAU Symp. #209, Planetary Nebulae: Their Evolution and Role in the Universe*. ASP, San Francisco, p.347
- Ruiz M. T. Peimbert A., Peimbert M., Esteban C., 2003, *ApJ*, 595, 247
- Schwarz H. E., Corradi R. L. M., Melnick J., 1992, *A&AS*, 96, 23
- Schlegel D. J., Finkbeiner D. P., Davis M., 1998, *ApJ*, 500, 525
- Sharpee B., Baldwin J. A., Williams R. E., 2004, *ApJ*, 65, 323
- Shklovsky I., 1956, *Astr.Zh.*, 33, 222
- Soker N., 1997, *ApJS*, 112, 487
- Storey P. J., Hummer D. G., 1995, *MNRAS*, 272, 41
- Tsamis Y. G., Barlow M. J., Liu X.-W., Danziger I. J., Danziger I. J., 2003a, *MNRAS*, 338, 687
- Tsamis Y. G., Barlow M. J., Liu X.-W., Danziger I. J., Storey P. J., 2003b, *MNRAS*, 345, 186
- Tsamis Y. G., Barlow M. J., Liu X.-W., Storey P. J., Danziger I. J., 2004, *MNRAS*, 353, 953
- Tylenda R., 2003, in S. Kwok, M. Dopita and R. Sutherland, eds. *IAU Symp. #209, Planetary Nebulae: Their Evolution and Role in the Universe*. ASP, San Francisco, p.389
- Wesson R., Liu X.-W., Barlow M. J., 2003, *MNRAS*, 340, 253
- Wesson R., Liu X.-W., Barlow M. J., 2005, *MNRAS*, 362, 424
- Williams R. E., Woolf N. J., Hege E. K., Moore R. L., Kopriva D. A., 1978, *ApJ*, 224, 171
- Zhang Y., Liu X.-W., Wesson R., Storey P. J., Liu Y., Danziger I. J., 2004, *MNRAS*, 351, 935
- Zhang Y., Liu X.-W., Liu Y., Rubin R. H., 2005a, *MNRAS*, 358, 457
- Zhang Y., Rubin R. H., Liu X.-W., 2005b, *RevMexAA (Serie de Conf.)*, 23, 15